

# Broad Recombination Line Objects in W49N on 600 AU Scales

C. G. De Pree<sup>1</sup>, D. J. Wilner<sup>2</sup>, A. J. Mercer<sup>1</sup>, L. E. Davis<sup>1</sup>, W.M. Goss<sup>3</sup>, S. Kurtz<sup>4</sup>

## ABSTRACT

High resolution 7 mm observations of the W49N massive star forming region have detected recombination line emission from the individual ultracompact (UC) HII regions on 50 milliarcsecond (600 AU) scales. These line observations, combined with multifrequency, high-resolution continuum imaging of the region at 7 mm (VLA) and at 3 mm and 1 mm (BIMA), indicate that five to seven of the eighteen ultracompact sources in W49N are broad recombination line objects (BRLOs) as described by Jaffe & Martin-Pintado (1999). BRLOs have both broad radio recombination lines ( $\Delta V > 60 \text{ km s}^{-1}$ ) and rising spectra ( $S_\nu \sim \nu^\alpha$ ), with  $\alpha$  values greater than 0.4. The broad line widths of the H52 $\alpha$  line are probably related to motions in the ionized gas rather than pressure broadening. A number of models have been proposed to explain the long lifetime of UC HII regions, including the photoevaporated disk model proposed by Hollenbach et al. (1994). This model can also explain the broad lines, rising spectra and bipolar morphologies of some sources. We suggest—based on line and continuum observations as well as source morphology—that in a subset of the W49N ultracompact sources we may be observing ionized winds that arise from circumstellar disks.

*Subject headings:* interferometry – nebulae: H II regions – nebulae: individual (W49N) – nebulae: internal motions

---

<sup>1</sup>Department of Physics and Astronomy, Agnes Scott College, 141 E. College Ave., Decatur, GA 30030

<sup>2</sup>Center for Astrophysics, 60 Garden Street, Cambridge, MA 02138

<sup>3</sup>National Radio Astronomy Observatory, P.O. Box 0, Socorro, NM 87801

<sup>4</sup>Centro de Radioastronomía y Astrofísica, UNAM, Morelia, Mexico

## 1. INTRODUCTION

The W49A star-forming region is among the most luminous in the Galaxy ( $10^7 L_{\odot}$ ) and is located within one of its most massive giant molecular clouds ( $10^6 M_{\odot}$ ). While W49A is a distant region (located at about 11.4 kpc), the large number, high luminosity and wide morphological variety of its HII regions make it a valuable region to study high mass star formation, as long as observations have sufficient angular resolution. The W49 North (W49N) cloud core within W49A contains over a dozen ultracompact (UC) HII regions powered by OB-type stars arranged in a 2 pc diameter ring (Dreher et al. 1984; Dickel & Goss 1990). The discovery of so many compact sources within W49N was one of the origins of the UC HII region "lifetime problem". That is, the observed number of UC sources seems to exceed the numbers expected based on a free expansion of the ionized gas (Dreher et al. 1984; Wood & Churchwell 1989). A variety of models have been proposed to account for this discrepancy, and were recently summarized in Jaffe & Martin-Pintado (1999; hereafter JMP).

A recent millimeter survey of UC HII regions (JMP) indicates that about 30% of them are characterized by (1) rising spectral indices ( $\alpha > 0.4$ ), and (2) broad radio recombination lines ( $\Delta V > 60 \text{ km s}^{-1}$ ), much broader than would be expected if the width were thermal ( $\sim 25 \text{ km s}^{-1}$ ). JMP refer to these sources as Broad Line Recombination Objects (BRLOs). In their analysis, JMP discuss the apparent correlation between spectral index values and radio recombination line (RRL) widths, summarize the existing models that could explain the correlation, and conclude that the disk-wind model (Hollenbach et al. 1994) is the most promising. Sewilo et al. (2003) have recently carried out a VLA survey of seventeen hypercompact (HC) HII regions, and report the detection of eight sources with H92 $\alpha$  or H76 $\alpha$  line widths greater than  $40 \text{ km s}^{-1}$ . They propose hierarchical clumping in the nebular gas as an explanation of the spectral indices observed. Here we describe new H52 $\alpha$  line observations that have uncovered a number of BLROs in W49N consistent with the 30%-50% of such sources found in these surveys. The scales probed by these observations ( $\sim 600 \text{ AU}$ ) may further clarify the nature of BRLOs, and provide new constraints for models of these young sources.

## 2. OBSERVATIONS AND RESULTS

We have undertaken an extensive high frequency, high resolution imaging and spectroscopy program in the massive star forming region W49A with the Very Large Array

(VLA)<sup>5</sup> (Wilner et al. 2001, De Pree et al. 2000, De Pree, Goss & Gaume 1998, De Pree, Mehringer & Goss 1997). Observations presented here have been taken over the past 6 years, with the most recent observations made in early April 2001. For the high resolution 7 mm images, we have combined continuum observations from 1995 (D configuration), 1998 (A configuration) and 2001 (B configuration). In the most recent B configuration observations, 7 mm receivers were present on 23 antennas, compared with only 12 in 1998 and 10 in 1995. The H52 $\alpha$  line has a rest frequency of 45.454 GHz, and all three observations were made in the 1A mode with 25 MHz bandwidth, centered at +8.0 km s<sup>-1</sup>. Data were Hanning smoothed by the on-line system, and spectra were separated into 15 channels, giving a channel separation and spectral resolution of 1.5625 MHz (10.3 km s<sup>-1</sup>).

Observations were carried out with the fast switching calibration technique. The nearby bright calibrator source J1925+2106 was used for both phase and bandpass calibration (for the line data). The A, B, and D configuration data sets were independently calibrated, combined with the AIPS task DBCON and the final continuum image was generated with the AIPS task IMAGR. Individual and combined continuum images were self-calibrated. The resolution of the final continuum image is 0''.055 x 0''.044, PA=11.5°, and the *rms* noise is 0.34 mJy/beam. The *rms* noise in the line channels is 1.7 mJy/beam. The corresponding resolution H52 $\alpha$  spectral line data set was reduced using standard techniques in AIPS.

Line parameters were generated from Gaussian fits to the data using the Groningen Image Processing System (GIPSY). Table 1 summarizes the results from the continuum and line data. Column (i) gives the source name, column (ii) indicates the peak line-to-continuum ratio, column (iii) gives the  $V_{LSR}$  of the H52 $\alpha$  line ( $\theta_{beam} \sim 0''.05$ ), column (iv) gives the H52 $\alpha$  line width from the high resolution data, column (v) gives the H52 $\alpha$  line width from the low resolution data (De Pree et al. 1997,  $\theta_{beam} \sim 1''.7$ ) and column (vi) gives the continuum spectral index. Spectral index values in this table are obtained using the 1.3 cm and 3 mm flux densities, except as noted (Wilner et al. 2001). Errors in the spectral indices, which are dominated by the absolute calibration of the continuum data, are  $\pm 0.1$ .

## 2.1. Continuum Images

The upper left panel of Figure 1 shows the 3.6 cm continuum emission from the central "ring" of HII regions in W49N (De Pree et al. 1997). Boxes labelled (i) to (iv) are the locations of the four insets that show the full resolution ( $\theta_{beam}=0''.05$ ) 7 mm continuum

---

<sup>5</sup>The National Radio Astronomy Observatory is a facility of the National Science Foundation operated under a cooperative agreement by Associated Universities, Inc.

emission from the ultracompact sources in W49N. The addition of the B configuration data has improved the 7 mm image quality over similar data presented by De Pree et al. (2000). In particular, the additional *uv* data provided by the 23 antennas in the B configuration aided in the deconvolution of the beam carried out by the AIPS task IMAGR.

We note that the interferometric 7 mm observations (even with the addition of the D configuration data) are missing flux density from emission on scales larger than about 40". The lower resolution imaging of W49A at 3.6 cm (De Pree et al. 1997) clearly shows the presence of emission on scales that are not imaged in the 7 mm observations. The comparison of these two images also emphasizes the way in which high frequency observations are biased toward the detection of high-density gas.

## 2.2. Line Data

Figure 2 shows the H52 $\alpha$  radio recombination line data and Gaussian fits from the 15 individual sources in W49N from which we detect line emission. Vertical bars in each spectrum indicate a 10% line-to-continuum ratio. Parameters from fits to the H52 $\alpha$  line are given in Table 1 as described above. Note that the bandwidth available with the current VLA correlator at this high frequency is just sufficient to detect the broadest lines, and in some cases, the line widths quoted may be lower limits. Six of the 18 continuum sources have H52 $\alpha$  lines broader than 40 km s<sup>-1</sup>, and four of these have lines broader than 50 km s<sup>-1</sup>. Three of the sources have no detected line emission (C1, E and G2c). In the case of C1 and E, the lack of a line detection may be due to limited sensitivity, since both sources are more extended, and source E has line emission detected at 3.6 cm (De Pree et al. 1997). In the case of G2c, a high emission measure source with a rising spectral index, the line may be too broad for the velocity coverage of the 7 mm observations with a total velocity range of 155 km s<sup>-1</sup>.

In Figure 2, sources G2a and G2b are shown with single Gaussian fits, and the parameters in Table 1 fit the line data with broad lines ( $\Delta V_{FWHM} > 50$  km s<sup>-1</sup>). Two Gaussian fits (not shown) indicate that these sources may be double peaked profiles, with line peak separations of about 33 km s<sup>-1</sup> and 38 km s<sup>-1</sup>, respectively. We note that in the two-component fits, the width of the individual peaks falls below 30 km s<sup>-1</sup>. The spectral resolution of these observations is insufficient to be conclusive, but certainly these objects should be reobserved when the new VLA correlator is available.

## 3. DISCUSSION

### 3.1. Spectral Indices and RRLs

The issue of impact broadening naturally arises in high density sources like ultracompact HII regions. Certainly, pressure (or impact) broadening is a significant effect in lower frequency ( $n > 100$ ) RRLs. However, the effect is strongly dependent on transition number ( $n$ ), and less strongly dependent on the electron density.

Using the equations presented in Brocklehurst & Seaton (1972), the ratio of pressure broadening ( $\Delta\nu^I$ ) to Doppler broadening ( $\Delta\nu^D$ ) is

$$\frac{\Delta\nu^I}{\Delta\nu^D} = 0.142 \left(\frac{n}{100}\right)^{7.4} \left(\frac{N_{e,true}}{10^4}\right) \quad (1)$$

where  $n$  is the transition number, and  $N_{e,true}$  is the true electron density. Using the canonical value for the density of an HII region ( $10^4 \text{ cm}^{-3}$ ), it is clear that pressure broadening is a small effect ( $\frac{\Delta\nu^I}{\Delta\nu^D} \ll 1$ ) for transitions with  $n < 100$ . Of course, the  $N_{e,rms}$  density value that we use will be lower than the true value ( $N_{e,true}$ ) in Eq. 1, dependent on the filling factor ( $\epsilon$ ). If the filling factor is small, and the true electron density ( $N_{e,true}$ ) much larger, then pressure broadening may become apparent at higher frequencies.

If the  $N_{e,true}$  value becomes larger than  $10^4 \text{ cm}^{-3}$ , and we set the ratio of  $\frac{\Delta\nu^I}{\Delta\nu^D}$  in Equation 1 equal to one, pressure broadening can become significant at smaller  $n$  values (higher frequencies). For example, at densities of  $10^6 \text{ cm}^{-3}$ , pressure broadening may become apparent at  $n=70$ . At densities of  $10^8 \text{ cm}^{-3}$ , even the H38 $\alpha$  line would experience pressure broadening.

For the H52 $\alpha$  line to be pressure broadened would require true electron densities in the range of  $10^7 \text{ cm}^{-3}$ . The broad line H52 $\alpha$  linewidths that are detected in W49N are from regions which have *rms* electron densities less than about  $10^6 \text{ cm}^{-3}$ , with most rms electron densities closer to  $10^5 \text{ cm}^{-3}$  (De Pree et al. 2000). For these densities, pressure broadening would only be a significant effect for  $n > 70$ . And even if the filling factor ( $\epsilon = (\frac{N_{e,rms}}{N_{e,true}})^2$ ) is as small as 0.01, pressure broadening would not be a factor at 45 GHz. However, if the filling factor is significantly smaller than 0.01, then the broad lines detected may be due to pressure broadening. The high resolution of these observations also eliminates another possible explanation of broad lines: the overlap of sources with different  $V_{LSR}$  values. Whatever the source of the broad lines, they arise from very compact regions ( $d \sim 600 \text{ AU}$ ).

It is possible to use the changing line width of the RRL lines as a function of frequency to determine a lower limit for the  $N_{e,true}$  for a particular source. For example, source D in W49N has a line width of  $48 \pm 1.6 \text{ km s}^{-1}$  at 3.6 cm,  $38.2 \pm 1.8 \text{ km s}^{-1}$  at 1.3 cm, and  $35.1 \pm 1.2 \text{ km s}^{-1}$  at 7 mm (De Pree et al. 1997). Using the 3.6 cm line width ( $48 \text{ km s}^{-1}$ )

for  $\Delta\nu^I$  and the 7 mm line width ( $35.1 \text{ km s}^{-1}$ ) for  $\Delta\nu^D$ , the lower limit for  $N_{e,true}$  is determined to be  $1.8 \times 10^5 \text{ cm}^{-3}$ , and the upper limit on the filling factor is  $\epsilon=0.1$ . If the other sources in W49N have similar filling factors, then pressure broadening is not likely to be the major contributor to broad lines in these sources.

### 3.2. Comments on Individual Sources

There are 18 individual sources identified in the 7 mm continuum image (see Table 1). Of these, six sources (A1, A2, B1, B2, G2a & G2b) have line widths greater than  $50 \text{ km s}^{-1}$ , and a seventh source with a rising spectral index (G2c) has no line detected, perhaps due to its large line width. Of the six sources with broad detected lines, four (B1, B2, G2a and G2b) have rising spectra, with  $\alpha > 0.8$ . Source A2 has a continuum spectral index of 0.3, and the fifth (A1) does not have a measured spectral index because only the 7 mm data has sufficient resolution and sensitivity to detect the source.

The W49A core has between five and seven sources with characteristics that would classify them as BLROs, as defined by JMP. In their millimeter survey, JMP found that approximately 30% of UC HII regions were BLROs, and we find a consistent ratio of BLROs in the W49N core.

#### 3.2.1. A Sources

Source A2 in W49N has ‘borderline’ BLRO characteristics (see Table 1). As has been discussed in De Pree et al. (2000), the morphology of source A2 is bipolar at lower resolution and frequency (3.6 cm image), and shell- or disk-like at higher resolution and frequency (7 mm image). Figure 1 shows the structures visible at different resolutions. The upper left panel shows the 3.6 cm data ( $\theta_{beam} \sim 0''.8$ ), and inset (i) shows the 7 mm continuum emission ( $\theta_{beam} \sim 0''.055$ ). Because the A configuration 7 mm data filters out large structures ( $>40''$ ), the bipolar lobes are less apparent in the higher frequency data. Source A is the most extended of the BLROs in W49N, and it may be near the end of its BLRO phase. However, it has a morphology and scale (see De Pree et al. 2000) that are consistent with the Hollenbach et al. (1994) photoevaporating disk model.

#### 3.2.2. G Sources

G1 and G1S are relatively extended, shell-like regions that have thermal line widths and continuum spectra consistent with an optically thin HII region. The G2a and G2b regions are located near the center of a high velocity molecular outflow traced in water maser emission (De Pree et al. 2000, McGrath et al. 2003), and both have broad ( $\Delta V > 50 \text{ km s}^{-1}$ ) radio recombination lines and rising spectral indices. For comparison, the thermal broadening of 10,000 K gas is  $21.4 \text{ km s}^{-1}$ . There is some indication that the lines in these two regions are multiple-peaked (see Fig. 2), but higher spectral resolution observations are required. The doubly peaked lines may be related to the high velocity outflow. The G2c source is bright and elongated, but has no detected H52 $\alpha$  line emission. The more extended G3, G4 and G5 sources (which seem to comprise portions of a large shell) have line widths that are consistent with thermal broadening, and spectral indices that are consistent with optically thin emission from ionized gas.

### 3.3. UCHII Region Models

JMP (1999) have reviewed the models currently proposed to explain the nature of UC HII regions. Originally these models were required only to explain the morphology and longevity of UC HII regions. Observations in JMP and this investigation have shown that about 30% of UC HII regions have other characteristics that must be explained by current models. These properties include spectral index values that are consistent with a constant velocity ( $\alpha=0.6$ ) or accelerating ( $\alpha > 0.6$ ) ionized wind, and broad ( $\Delta V_{FWHM} > 60 \text{ km s}^{-1}$ ) radio recombination lines. In addition to the models reviewed in JMP, De Pree et al. (1995b) have suggested that pressure confinement might explain the longevity of some UC HII regions, and Keto has described a gravitationally bound hypercompact HII region model that may also be relevant (Keto 2002a, 2002b). Most recently, Sewilo et al. (2003) have suggested that the rising spectral indices detected in their HC HII region survey could be explained by hierarchical clumping of nebular gas.

In their discussion, JMP conclude that while none of the models in their current form fully explain the new observations, the mass-loaded wind (Dyson, Williams & Redman 1995) and the disk wind models (Hollenbach et al. 1994) are the most promising. As they point out, these two models can potentially account for the UC HII region lifetime problem. In addition, the disk wind model can explain the  $r^{-2}$  or steeper density gradients that are suggested by the rising continuum spectral indices, though other models (including champagne outflow) could potentially account for this density profile. Recent observational evidence for the presence of disks around high mass stars may support the disk wind model. For example, near-IR observations (Conti & Blum 2002) suggest that hot, dense disks might be present in the environments of very young massive stars in W49N. In addition,

the clearly bipolar structure of source A2 in W49N observed at low frequencies (3.6 cm, see Fig. 1) is shown to have a morphology consistent with an inclined 'disk' at high frequencies (7 mm, see Fig. 1 inset (i)). While sources with bipolar and disk morphologies are not widespread, the combined ring/bipolar morphology in source W49N:A2 suggests that a remnant accretion disk might be present in this source.

#### 4. CONCLUSIONS

High resolution, high frequency line and continuum observations of the W49N region indicate that broad radio recombination line widths detected on small scales at 1.3 cm persist at 7 mm. In addition, we have detected line emission from four sources (A1, B1, B3 & G1S) unresolved in previous H52 $\alpha$  RRL observations of W49N (De Pree et al. 1995a). Six ( $\pm 1$ ) of the 18 continuum sources in the W49N core have characteristics that would classify them as BLROs, roughly in agreement with the 30% value found in the JMP survey of UC HII regions. Broad lines in these regions detected at 7mm are likely to have a kinematic origin. The new RRL observations clearly provide a discriminating factor between BRLOs and normal UC HIIs in this massive star forming region.

CGD acknowledges the support of NSF grant AST-0206103, and Jewels Deblasio for a careful reading of the manuscript. DJW and CGD thank NRAO for hospitality in Socorro, NM where some of this work was carried out. SK acknowledges the CONACyT grant 36568-E and DGAPA grant IN118401.

## REFERENCES

- Brocklehurst, M., & Seaton, M.J. 1972, MNRAS, 157, 179
- Conti, P.S. & Blum, R.D. 2002, ApJ, 564, 827
- De Pree, C.G., Dickel, H.R., Rodríguez, L.F. & Goss, W.M. 1995a, ApJ, 447, 220
- De Pree, C.G., Rodríguez, L.F., & Goss, W. M. 1995b, RMxAA, 31, 39
- De Pree, C.G., Mehringer, D.M. & Goss, W.M. 1997, ApJ, 482, 307
- De Pree, C.G., Goss, W.M., & Gaume, R.A., 1998, 500, 847
- De Pree, C.G., Wilner, D.J., Goss, W.M., Welch, W.J., & McGrath, E. 2000, ApJ, 540, 308
- Dickel, H. R., and Goss, W. M. 1990, ApJ, 351, 189
- Dreher, J.W., Johnston, K.J., Welch, W.J., & Walker, R.C. 1984, ApJ, 283, 632
- Dyson, J.E., Williams, R.J.R., & Redman, M.P. 1995, MNRAS, 277, 700
- Hollenbach, D., Johnstone, D, Lizano, S. & Shu, F. 1994, ApJ, 428, 654
- Jaffe, D. T. & Martin-Pintado, J., 1999, ApJ, 520, 162
- Keto, E. 2002a, ApJ, 568, 754
- Keto, E. 2002b, ApJ, 580, 980
- McGrath, E., Goss, W.M. & De Pree, C.G. 2003, in preparation
- Sewillo, M., Churchwell, E., Kurtz, S., Goss, W.M. & Hofner, P. 2003, submitted to ApJ
- Wilner, D. J., De Pree, C. G., Welch, W. J., Goss, W. M., 2001, ApJ, 550, 81
- Wood, D. O. S., & Churchwell, E. 1989, ApJS, 69, 831

Source (W49N)	$\frac{T(L)}{T(C)}$	$V_{LSR}$ (km/s)	$\Delta V_{HiRes}$ (km/s)	$\Delta V_{LowRes}$ (km/s)	$\alpha$ ( $S_\nu \propto \nu^\alpha$ )
A1	0.31±0.05	11.5±3.9	61±15	. . .	. . .
A2	0.28±0.03	15.4±1.8	43.4±5.4	47±2	0.3
B1	0.22±0.03	11.2±3.2	64±13	. . .	1.1
B2	0.21±0.02	16.8±1.9	43.9±5.8	49±3	0.9
B3	0.09±0.03	25.1±4.7	25±12	. . .	. . .
C	0.40±0.02	−8.0±0.7	32.4±1.8	39±3	0.1
C1	<0.50				
D	0.73±0.07	6.5±1.3	28.6±3.4	35±1	-0.1
E	<0.50				
F	1.3±0.2	3.9±2.3	29.2±6.1	26±1	-0.1
G1	0.57±0.05	2.9±1.1	29.2±2.9	. . .	0.3
G1S	0.94±0.1	14.2±1.7	24.1±4.5	. . .	0.0 <sup>a</sup>
G2a	0.08±0.01	6.2±4.3	59±10	40±1	1.1
G2b	0.13±0.03	22.8±5.7	58±14	. . .	0.8
G2c	<0.05				0.9 <sup>a</sup>
G3	1.30±0.04	11.2±0.5	32.4±1.2	. . .	0.2 <sup>b</sup>
G4	1.60±0.09	9.4±0.8	27.7±2.0	34±1	0.2 <sup>b</sup>
G5	1.0±0.2	9.0±2.8	38.7±7.8	. . .	0.2 <sup>b</sup>

Table 1: H52 $\alpha$  Line Properties and Spectral Indices

<sup>a</sup>Spectral index between 7 mm and 3 mm

<sup>b</sup>Spectral index between 3.6 cm and 3 mm

Fig. 1.— Upper left pseudocolor image shows the 3.6 cm radio continuum toward W49N (from De Pree et al. 1997). Boxes numbered (i) through (v) indicate the regions of detail showing the 7 mm radio continuum. The resolution of the 3.6 cm data is  $\sim 0''.8$ , and the resolution of the 7 mm data is  $0''.055 \times 0''.044$  ( $\sim 500$  AU). Insets show (i) W49N:A1 and A2, (ii) W49N:B1, B2 and D, (iii) W49N:C, (iv) W49N:G1, G2a, G2b and G2c, and (v) W49N:G3. Offsets are from the phase center of the 7 mm VLA observations ( $\alpha$  19 10 12.916,  $\delta$  09 06 11.916). The contour levels are at -1, 1, 1.4, 2, 2.8, 4, 5.6, 8, 11.2, 16, 22.4, 32, and 44.8 times a  $5\sigma$  level of  $1.7 \text{ mJy beam}^{-1}$ .

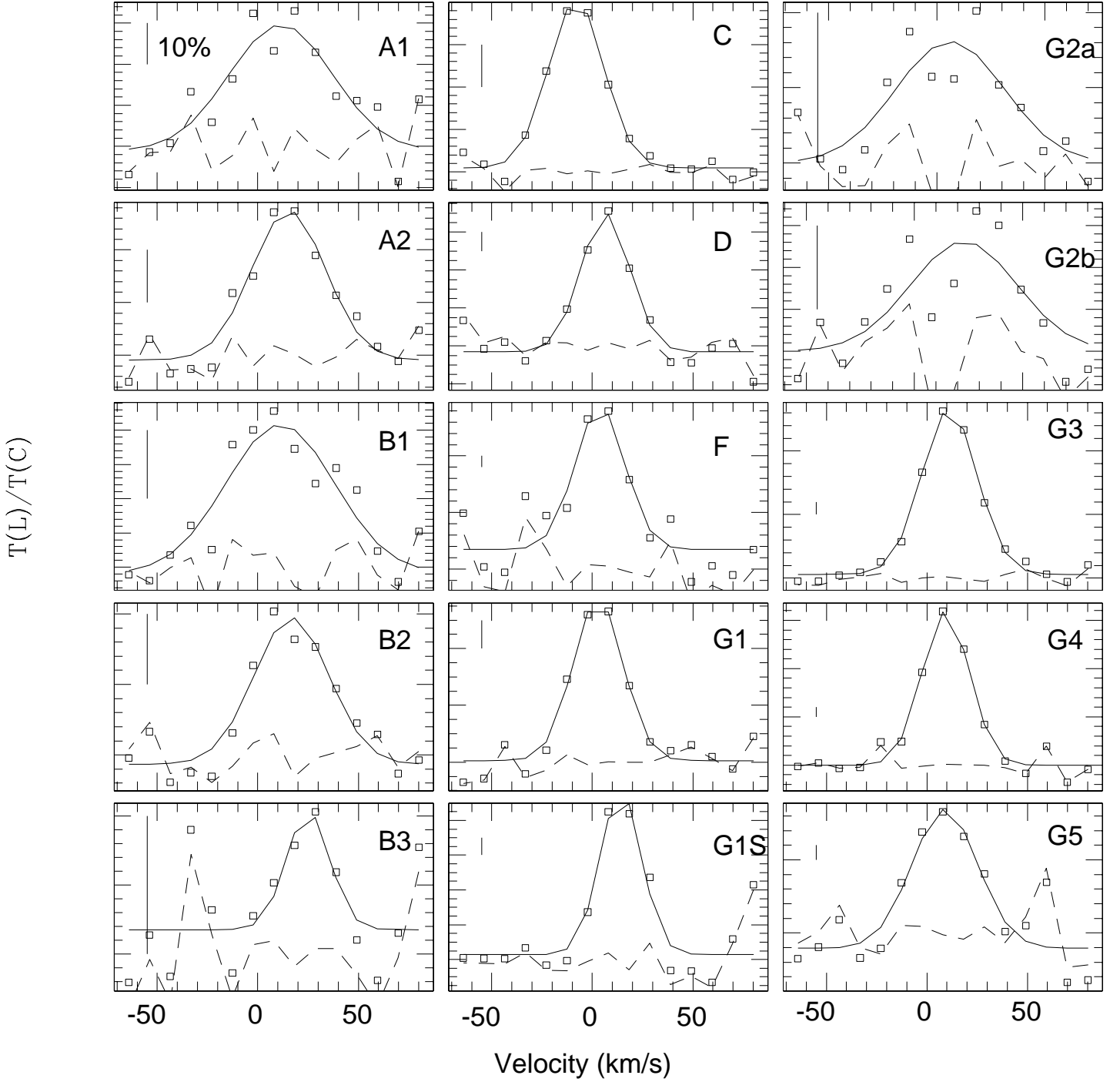


Fig. 2.— H52 $\alpha$  (45.4 GHz) radio recombination lines from the individual sources. Plots show the data (open squares), single Gaussian fit (solid line) and residual (dashed line). The parameters of the fits are given in Table 1. Vertical scale indicates line-to-continuum ratio, and the vertical line in each plot indicates 10%.

This figure "fig1.gif" is available in "gif" format from:

<http://arXiv.org/ps/astro-ph/0311417v1>